Nitrogen adsorption *via* charge transfer on vacancies created during surfactant assisted exfoliation of TiB$_2$

Anshul Rasyotra[a], Anupma Thakur[a], Raviraj Mandalia[b], Raghavan Ranganathan[b] and Kabeer Jasuja[a*]

[a] *Discipline of Chemical Engineering, Indian Institute of Technology Gandhinagar, Palaj, Gandhinagar, Gujarat 382055, India*

[b] *Discipline of Materials Engineering, Indian Institute of Technology Gandhinagar, Palaj, Gandhinagar, Gujarat 382055, India*

Corresponding Author: kabeer@iitgn.ac.in

Electronic Supplementary Information (ESI)

A. Crystal Structure of Titanium Diboride (TiB$_2$)
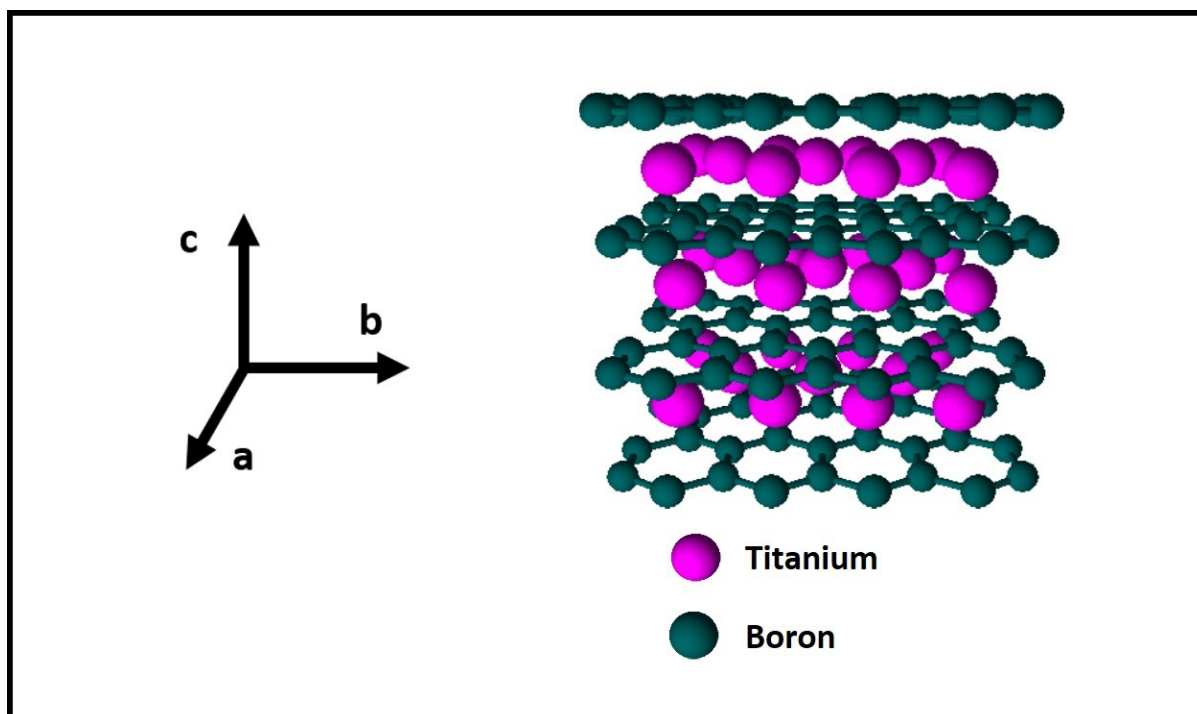
Figure S1*: **Crystal structure of TiB$_2$** – pink-colored atoms represent titanium, and green-colored atoms represent boron.*

TiB$_2$ is a well-known ceramic material with high mechanical strength and wear resistance. It has a hexagonal C32 structure with P6/mmm space group. TiB$_2$ has primarily been used as a coating for aluminium electrolysis cell, as a cutting tool, or as a conductive ceramic material. However, nano scaling this metal diboride opens up various avenues when the chemistry of boron and transition metal atoms could be used for various energy applications.

Table S 1: *Lattice parameters of TiB$_2$*

| Lattice parameters	Atomic distance (Å)
a	3.03
b	3.03
c	3.23

B. Pre-Treatment of Bulk TiB$_2$ Powder
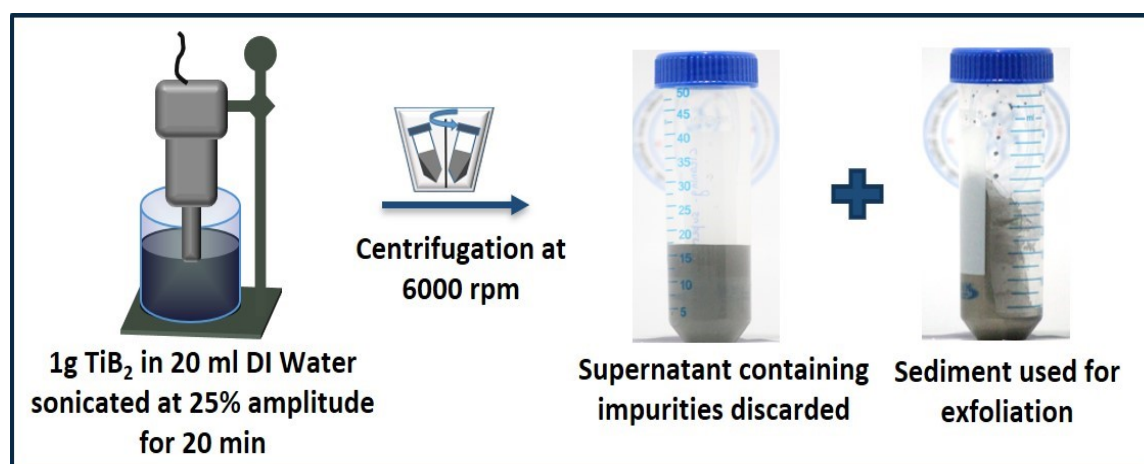
Figure S 2: *Procedure for cleaning of bulk TiB$_2$ powder*

1 gm of TiB$_2$ bulk powder (Sigma Aldrich, 99% pure, size < 10 μm) was added to 20 mL of deionized water (Millipore Ultrapure Type - II, ionic conductivity = 18.2 MΩ·cm (25℃)) at a concentration of 50 mg/mL. The mixture was probe sonicated for 20 minutes at 25% amplitude using QSonica 500 probe sonicator. This step was performed to remove any impurities in the as-obtained powder.

C. Tyndall Effect
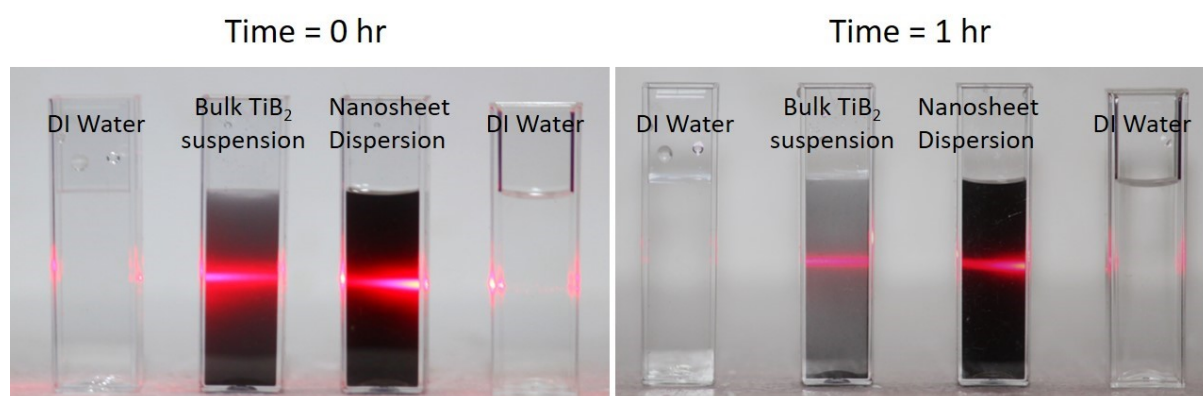
Figure S 3: Tyndall effect test to check the colloidal nature of the dispersion.

At t = 0 hr, both bulk TiB_2 suspension and TiB_2 nanosheet dispersion having different color shows Tyndall effect. After 1 hr, much of the bulk TiB_2 powder settles at the bottom which is apparent from the color of the solution. However, no color change in TiB_2 nanosheet dispersion indicates better stability compared with bulk TiB_2 suspended in DI water. The appearance of beam in bulk TiB_2 suspension is possibly due to the impurities in the bulk powder which are cleaned during the pre-treatment step as explained in Figure S2.

D. Surfactant removal and Recovery of powder form of nanosheets

In this process, nanosheets were centrifuged at 14500 RPM for 10 min. The supernatant was discarded and the sediment was redispersed in 20 mL of DI water. This dispersion was
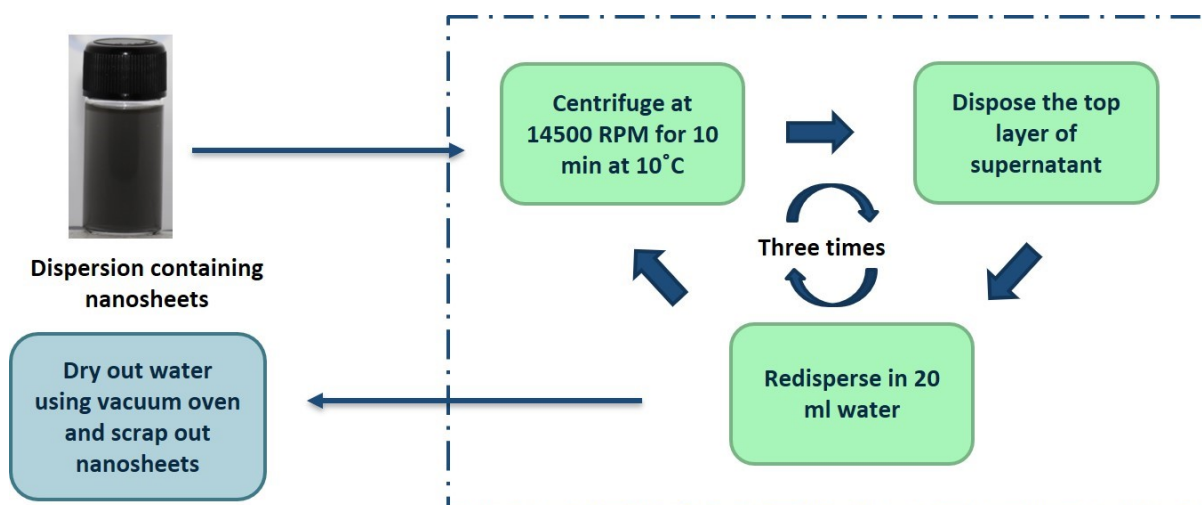

Figure S 4: Recovery of nanosheets in powder form

centrifuged at 14500 RPM to settle out the nanosheets. This procedure was repeated three times to remove the surfactant from the nanosheets. The final sediment was then kept for drying in a vacuum oven for 2 hours at 60°C.

E. Choice of the centrifugation rate

A 100 ml dispersion of TiB_2 nanosheets was prepared and divided into four parts of 25 mL each. This dispersion was subjected to different centrifugation rates – 1000 RPM, 1500 RPM, 2000 RPM, and 3000 RPM for 45 minutes. ~ 15 mL supernatant from each dispersion was collected and drop cast on the lacey carbon Cu grid (300 mesh) for TEM analysis. TEM images for all four dispersions are shown below. The centrifugation rate of 1500 RPM was chosen because the dispersion obtained after centrifugation at 1000 RPM contained some unexfoliated crystallites. The centrifugation rate of 1500 RPM removed all the unexfoliated crystallites in the dispersion. The higher centrifugation rate would have resulted in the loss of nanosheets with large lateral sizes.

1000 RPM
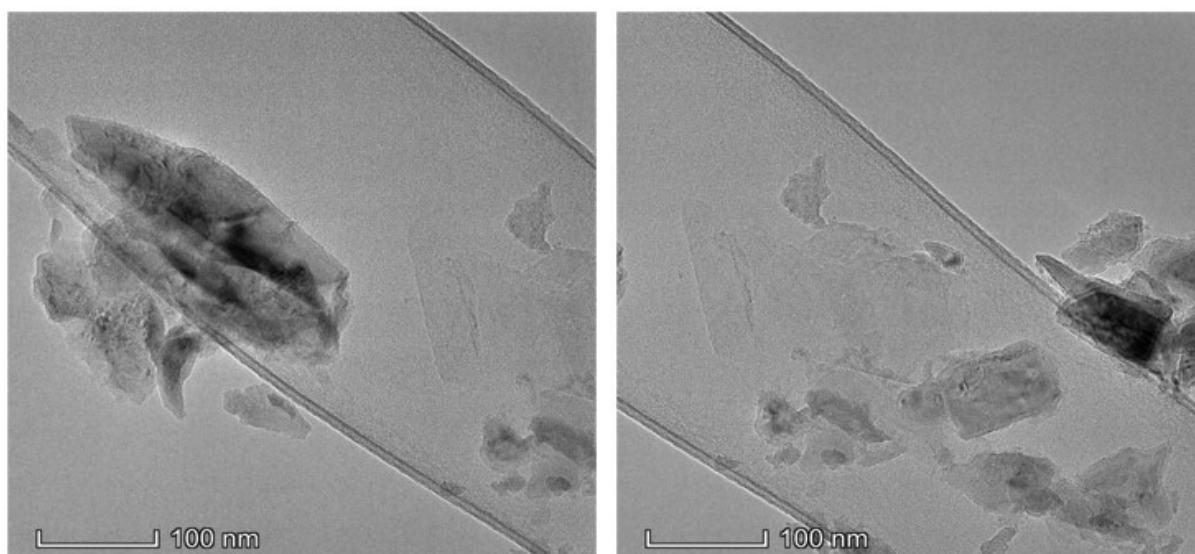
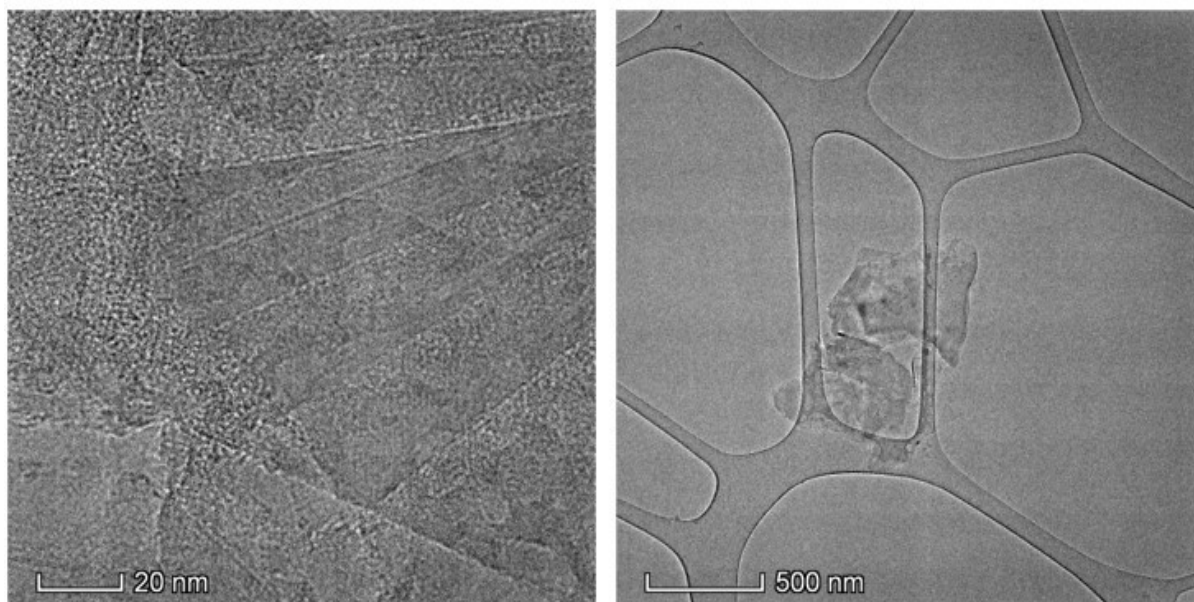***Figure S 5:*** *TEM images of nanosheets obtained after centrifuging the dispersion at 1000 RPM*

1500 RPM
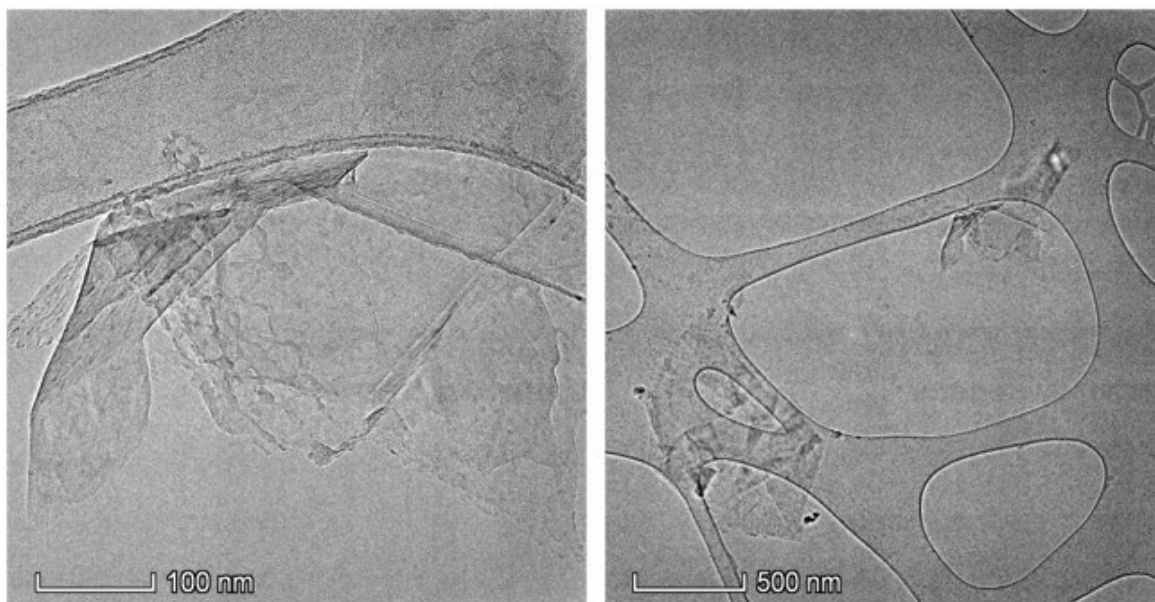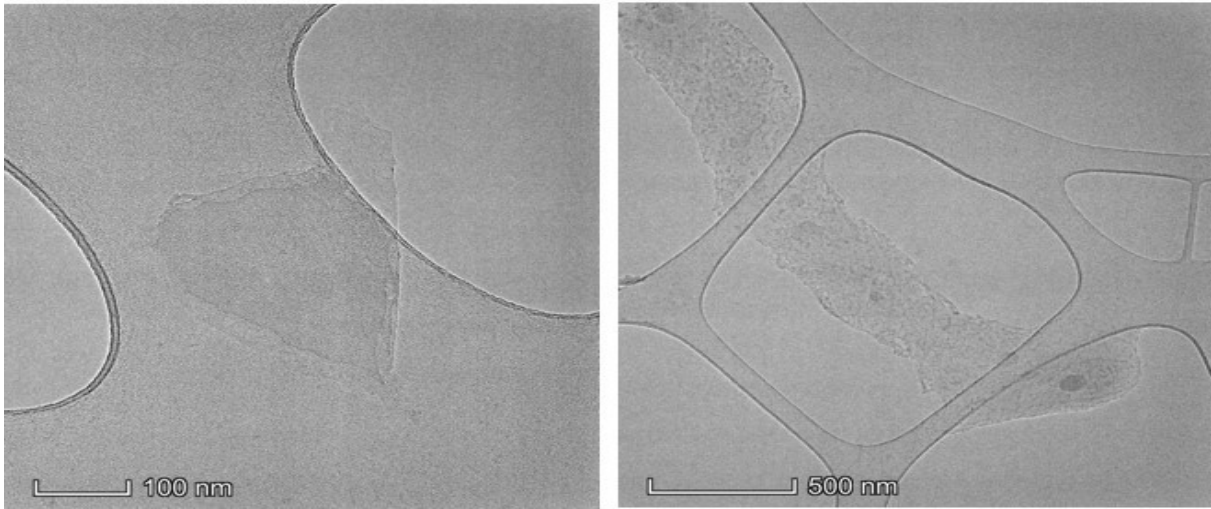

Figure S 6: *TEM images of nanosheets obtained after centrifuging the dispersion at 1500 RPM*

2000 RPM

Figure S 7: *TEM images of nanosheets obtained after centrifuging the dispersion at 2000 RPM*

3000 RPM

Figure S 8: *TEM images of nanosheets obtained after centrifuging the dispersion at 3000 RPM*

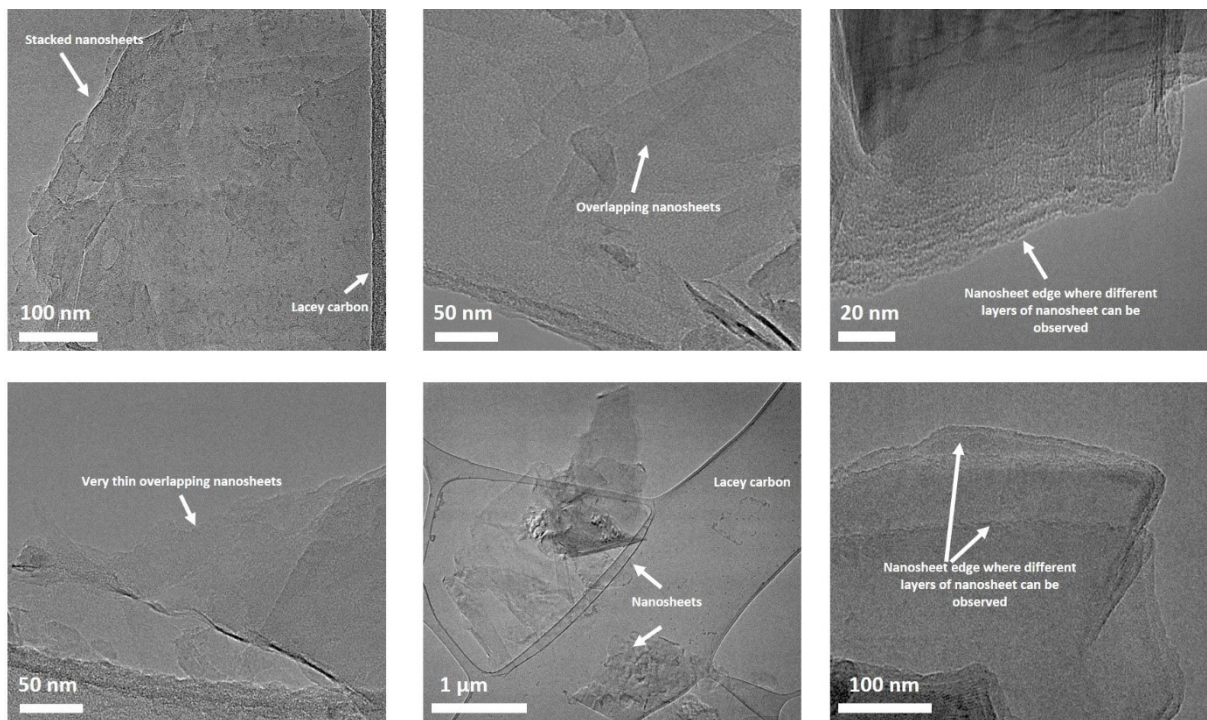## F. TEM Library:

Figure S 9: *TEM images of nanosheets obtained from r = 0.2*
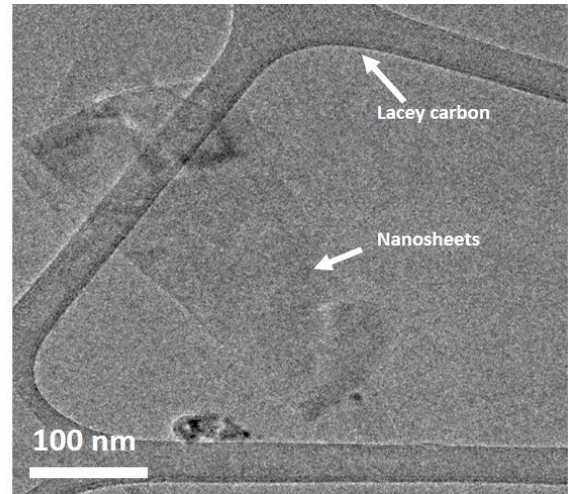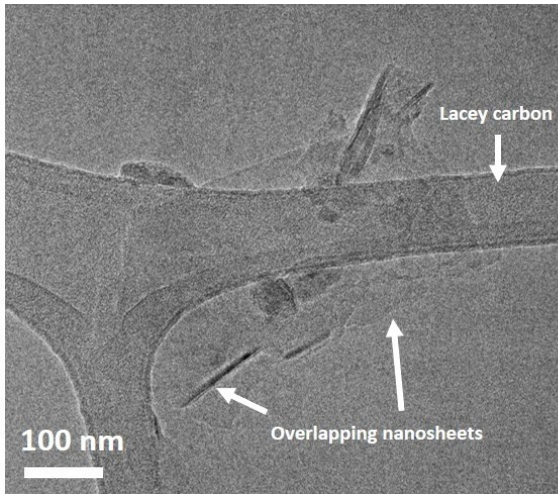
Figure S 10: *TEM images of nanosheets obtained from r = 0.1*
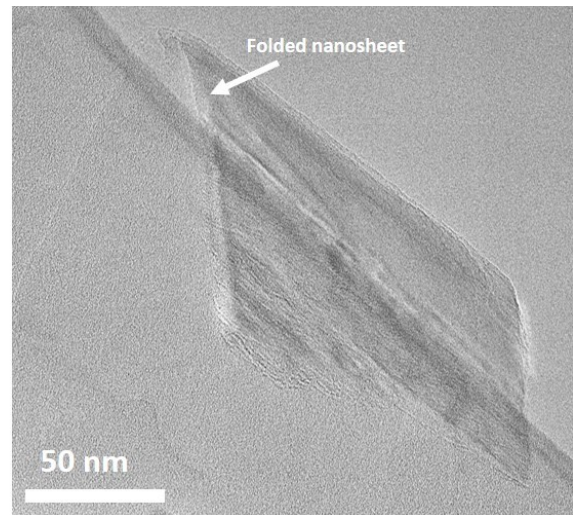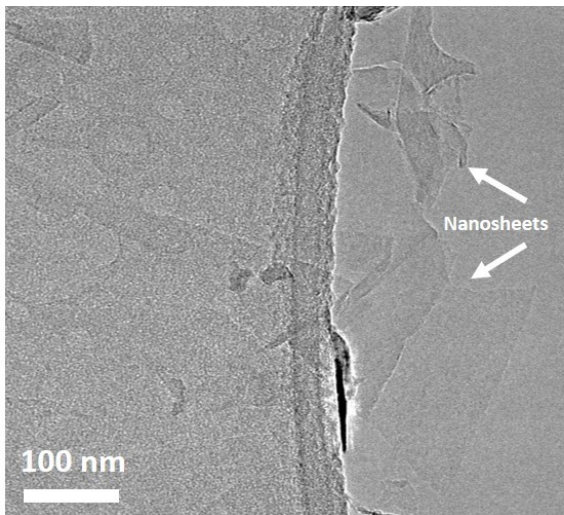
Figure S 11: *TEM images of nanosheets obtained from r = 0.15*
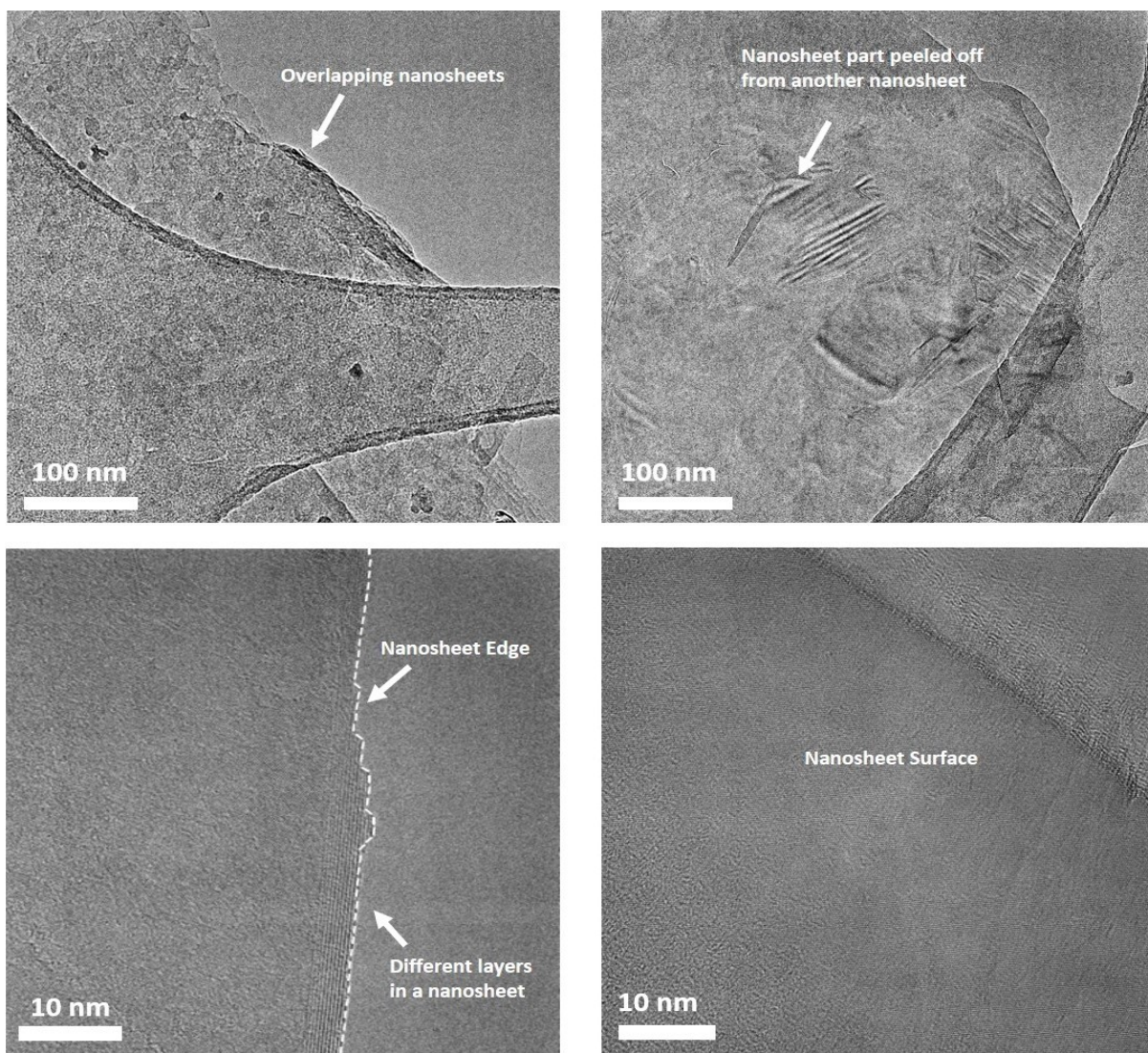
Figure S 12: *TEM images of nanosheets obtained from r = 0.3*
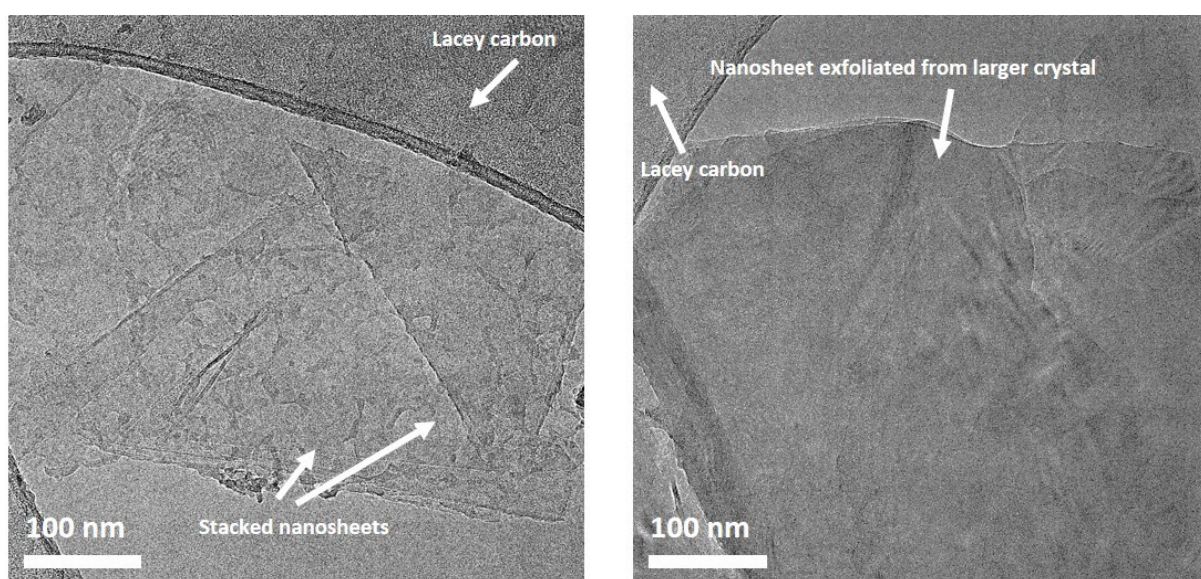
Figure S 13: *TEM images of nanosheets obtained from r = 0.4*

Figure S 14: *Different patterns observed due to overlapping nanosheets*

a)

b)
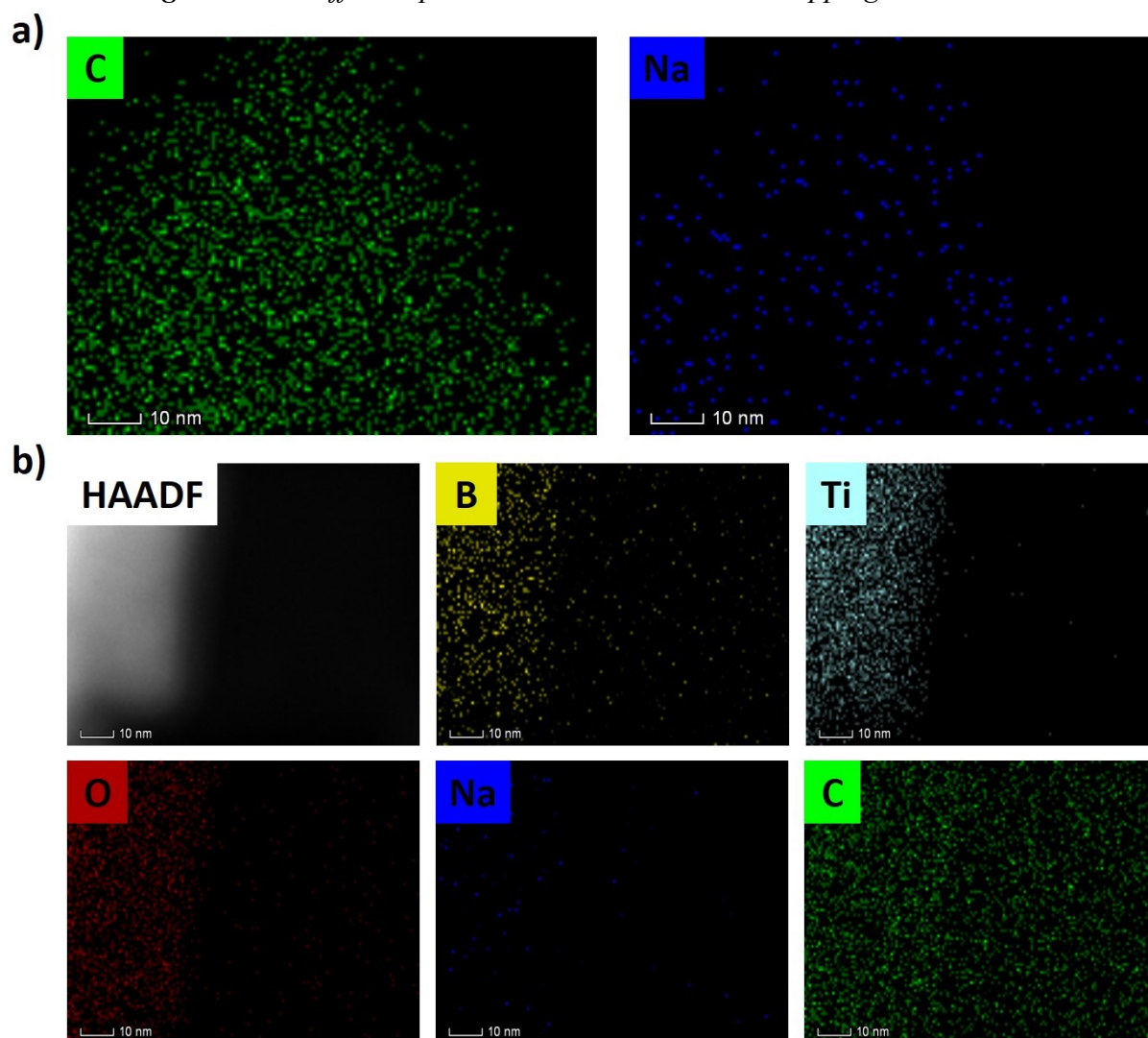
Figure S 15: *TEM-EDS mapping of nanosheets. (a) Carbon and sodium signal captured from the nanosheet in Figure 2(e) in the main manuscript. (b)EDS mapping of a different nanosheet.*

two overlapping nanosheets
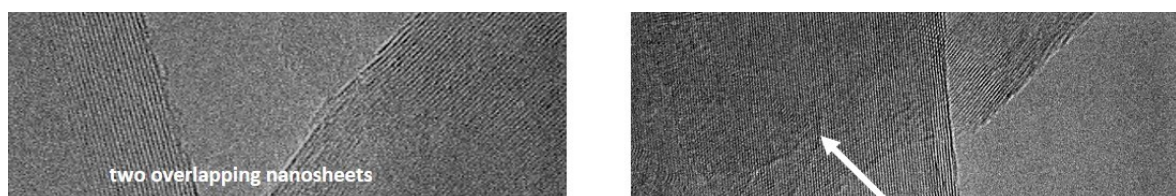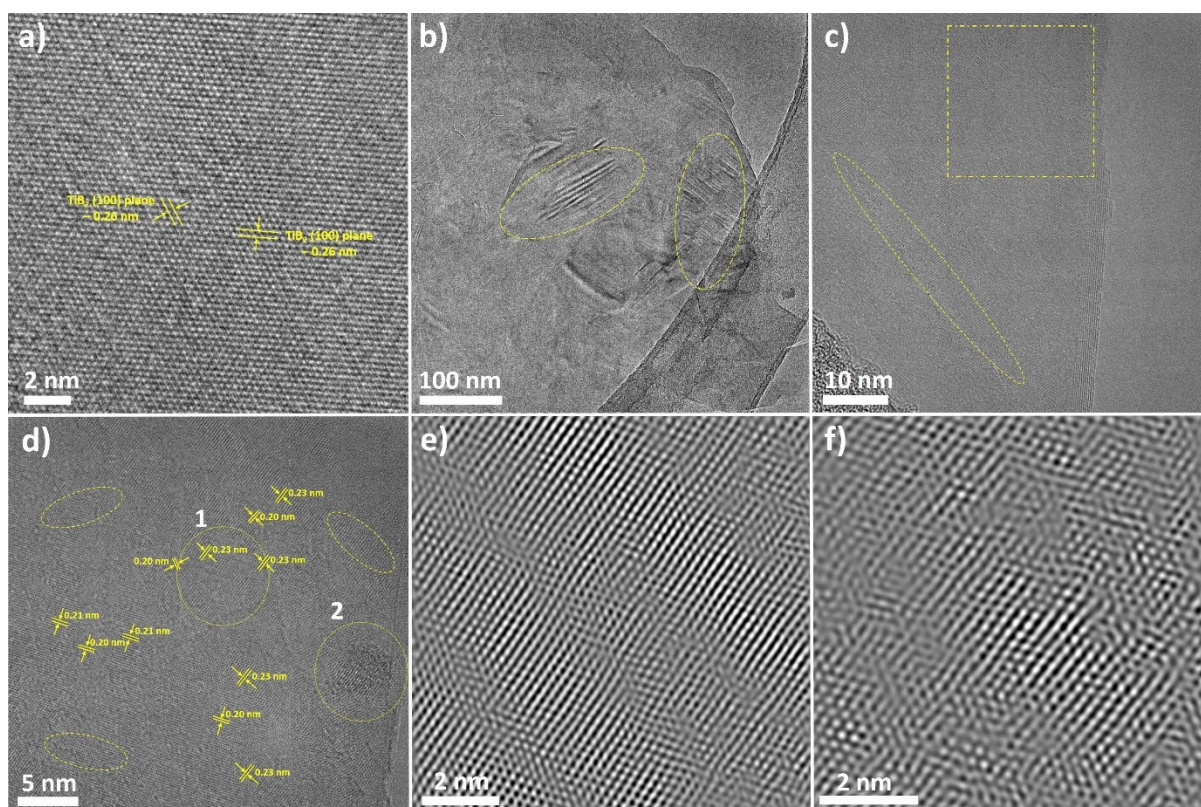
Figure S 16: *(a) HRTEM image of the selected area from Figure 2g having no defects and d-spacing of 0.20 nm corresponding to (101) plane of TiB_2. (b) TEM image of a nanosheet where defects are clearly visible indicated using yellow eclipse. (c) HRTEM image of a different nanosheet shows a line defect (indicated using yellow eclipse) present on the plane along with multiple small defects. (d) HRTEM image of marked area of Figure 1c showing various defects. (e,f) Inverse FFT image of marked area 1 and 2 in Figure 1d showing defect-rich regions.*

Figure S16a represents a magnified version of Figure 2h from the main manuscript where d-spacing of 0.26 nm was obtained directly and matches with (101) plane of TiB_2. Figure S16b presents an HRTEM image of a different nanosheet where the defects are clearly visible. Figure S16c presents a third nanosheet where a line defect is clearly visible with multiple small defects. Figure S16d is a magnified version of Figure S16c where different defects have been marked using yellow eclipse. We also compared the d-spacings from defect-free regions and regions where defects were observed within in the same nanosheet. A d-spacing of 0.20 nm was obtained from defect-free region which corresponds to (100) plane of TiB_2. Similarly, d-spacings of 0.22 nm and 0.23 nm were obtained from regions where defects were clearly visible. This increase in interlayer spacing is possibly due to the incorporation of oxygen or nitrogen functional groups in the TiB_2 lattice.[1] We further generated an inverse FFT image

from circular region 1 and 2 in Figure S16d to clearly view the defects which is presented as Figure S16e, f. The inverse FFT image clearly shows the presence of defects over the nanosheet area. Zhang *et al.* inferred a similar increase in the interlayer spacing of regions having defects in MoS_2 nanosheets.[2]

G. Identifying (hkl) plane from SAED pattern image:

To identify the (hkl) planes, ImageJ software was used. The scale bar in the SAED image was used to calibrate the lengths in the software. The distances between various spots were noted down by plotting circles over various planes in the image and noting down their diameters represented by 1/2r or 1/d. Here, "d" refers to the interplanar distance. Further calculations have been shown below in the table. (hkl) values were taken from ICDD database corresponding to the d-spacing values.

Table S 2: Calculations for determining (hkl) planes in SAED image

S. No.	1/2r or 1/d (nm⁻¹)	1/r (nm⁻¹)	r (nm)	d (Å)	(hkl)
1	12.42	6.21	0.161	1.61	(002)
2	9.85	4.925	0.203	2.03	(101)
3	7.81	3.905	0.256	2.56	(100)
4	6.32	3.16	0.316	3.16	(001)

H. Histogram for determining the average thickness of the nanosheets

Average thickness = 6 nm
Median thickness = 4 nm
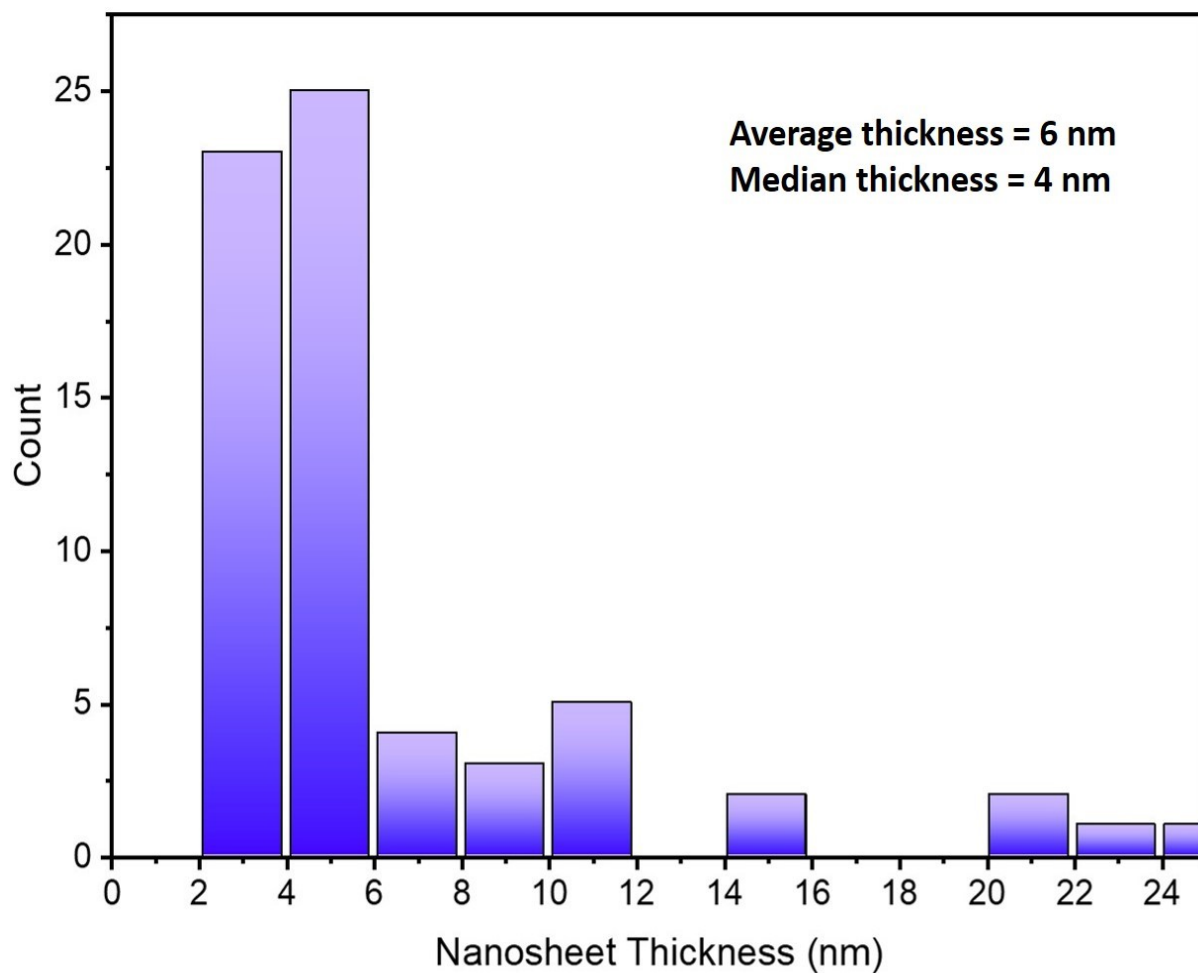
Figure S 17: Histogram representing the thickness corresponding to the exfoliated nanosheets

I. UV-Vis Plots

Figure S 18: *UV-Vis plot of TiB$_2$ nanosheets dispersion at different concentration*
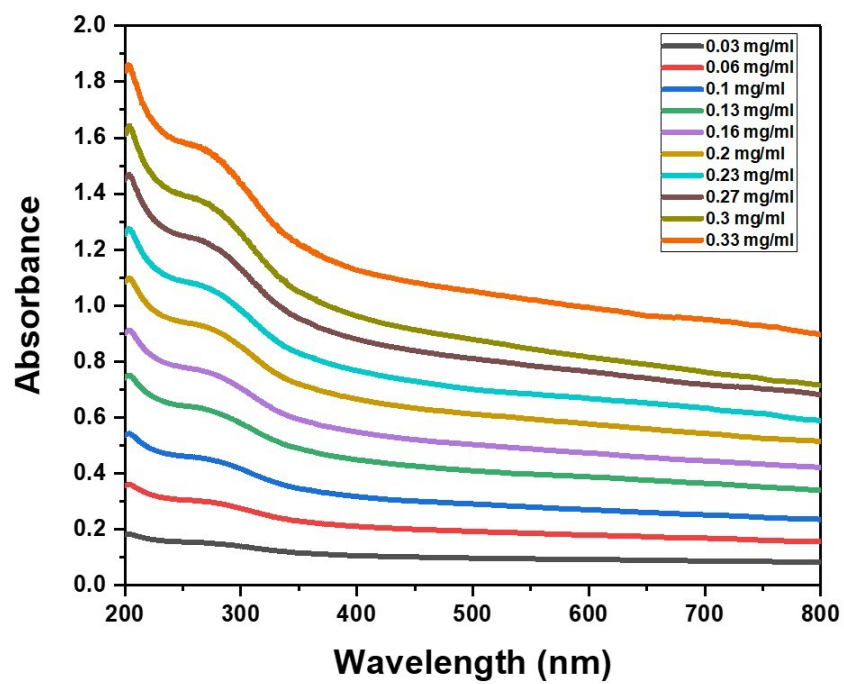
J. Raman Spectra:

Figure S 19: *Raman spectra of bulk TiB₂ and TiB₂ nanosheets*

K. XPS Results

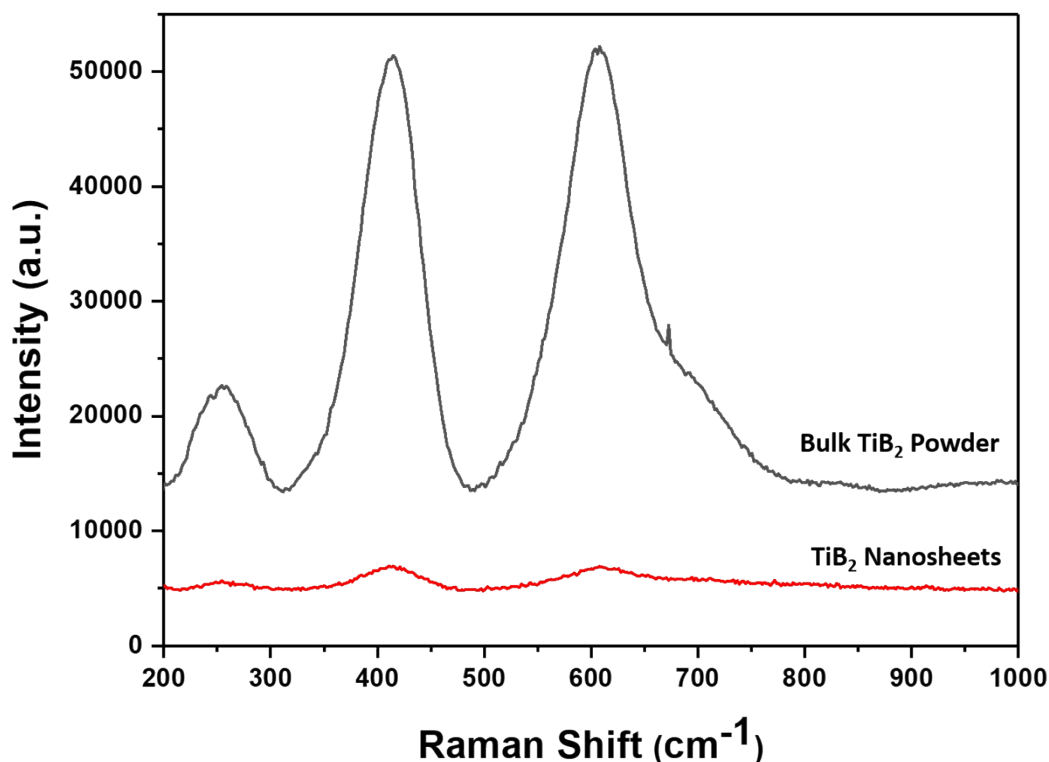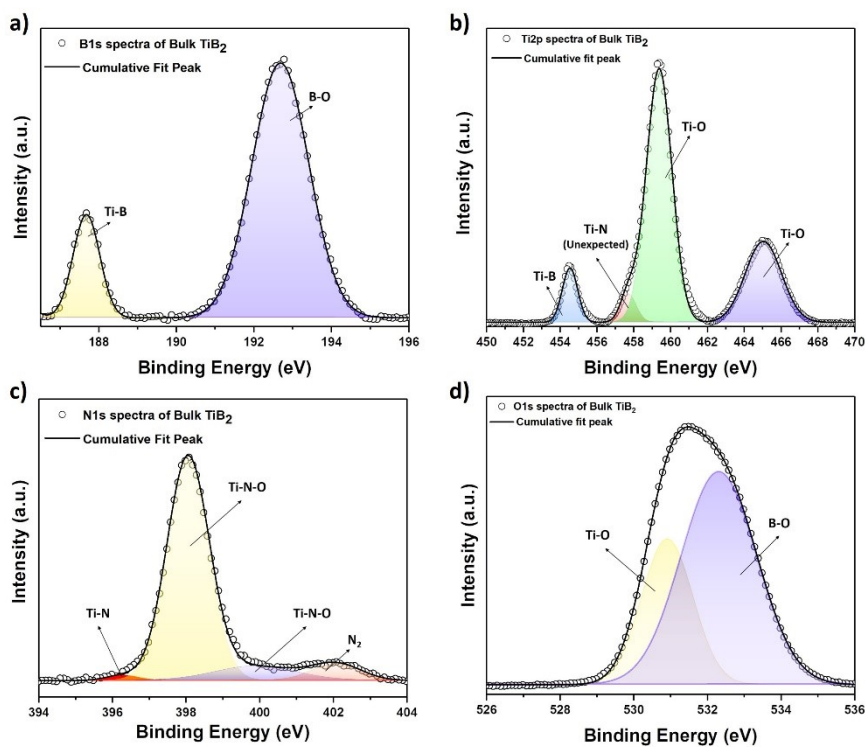Figure S20a depicts B1s spectra of bulk TiB_2. B1s spectrum of bulk TiB_2 shows two peaks – 187.68 eV (characteristic peak attributed to Ti-B bond) and 192.68 eV (attributed to B-O bond from B_2O_3). Ti 2p spectrum obtained from bulk TiB_2 exhibits four peaks - one centered at 454.5 eV (Ti-B bond), two centered at 459.3 eV and 465.1 eV, attributed to $2p_{3/2}$ and $2p_{1/2}$ modes of Ti respectively, indicating presence of Ti-O bond[3,4] and fourth centered at 457.5 eV corresponding to Ti-N bond (Figure S20b). The mechanism of adsorption of N_2 by bulk TiB_2 is shown in DFT studies section where Ti atoms are solely responsible. This is corroborated by XPS results shown below. N1s spectra of bulk TiB_2 exhibits four peaks – 396.5 eV, 397.6 eV. 400 eV, and 402 eV (Figure S20c). The peaks at 396.5 eV and 397.6 eV is attributed to the presence of TiN and Ti-N-O respectively. The peak at 400 eV is attributed to oxynitrides of transition metals and peak at 402 eV corresponds to adsorbed N_2. O1s spectra of bulk TiB_2 also show two peaks at 530.9 eV and 532.31 eV, with the former peak being attributed to titanium dioxides and the latter being attributed to boron oxides (Figure S20d).[3,5] The presence of B-O bond indicates oxygen species is present even in bulk TiB_2 indicative of surface functionalization.[3,5,6] In a study involving exfoliation of graphite, Skaltas and co-workers explained that oxygenated species are induced on the nanosheet lattice due to the defects

generated during ultrasonication.[7] Coleman and co-workers' explanation of the exfoliation mechanism further supported this defect generation[8]. We anticipate a similar phenomenon at play here. However, defects can be present even in bulk crystals and accompanied by oxygen species. This implies that while it is possible to minimize surface modification, presence of functional groups on the surface is unavoidable.

Figure S 20: *(a)B1s spectra, (b) Ti2p spectra, (c) N1s spectra, and (d) O1s spectra of bulk TiB$_2$ acquired by XPS*
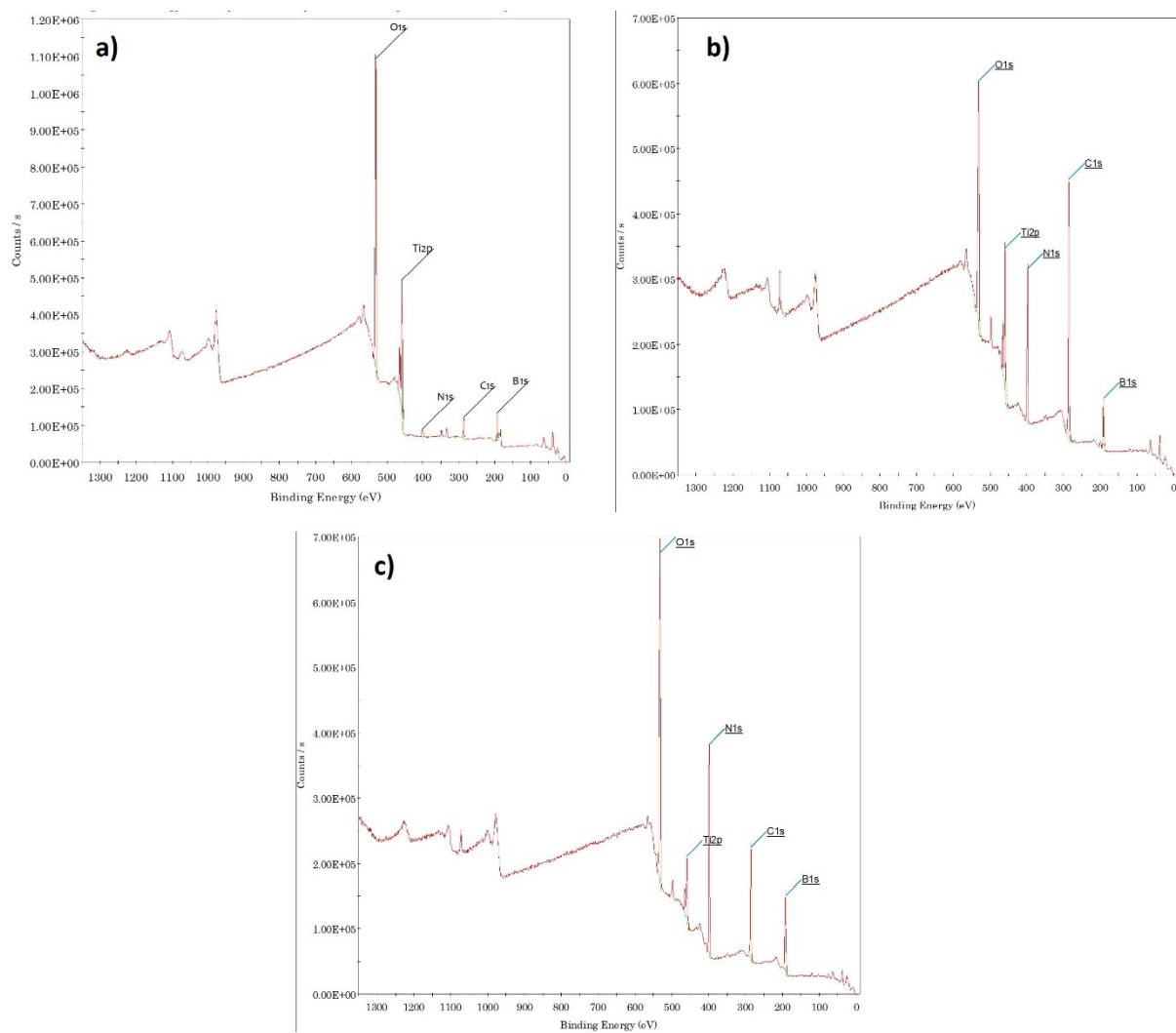
Figure S 21: *XPS survey scan of (a) bulk TiB$_2$, (b) TiB$_2$ nanosheets, and (c)TiB$_2$ nanosheets after TGA as obtained from the instrument*

L. ICP-AES Analysis

Table S 3: *Stoichiometric ratio of Ti and B in the bulk TiB$_2$ and nanosheets obtained using ICP-AES analysis*

Sample	ICP-AES Value (mg l^{-1})		Stoichiometric ratio
	Ti	**B**	**Ti:B**
Bulk TiB$_2$			
1	36.356	17.603	0.93:2
2	35.463	17.095	0.93:2
3	43.092	20.921	0.93:2
r = 0.1; Surfactant Concentration = 1 g/l; Initial Bulk TiB$_2$ Powder = 10 g/l			
1	0.231	0.307	0.34:2
2	0.263	0.545	0.22:2
3	0.251	0.552	0.21:2
r = 0.15; Surfactant Concentration = 1.5 g/l; Initial Bulk TiB$_2$ Powder = 10 g/l			
1	1.161	1.249	0.42:2
2	0.720	0.835	0.39:2
3	0.585	0.601	0.44:2
r = 0.2; Surfactant Concentration = 2 g/l; Initial Bulk TiB$_2$ Powder = 10 g/l			
1	0.704	0.451	0.7:2
2	0.718	0.562	0.58:2
3	0.771	0.607	0.57:2
r = 0.3; Surfactant Concentration = 3 g/l; Initial Bulk TiB$_2$ Powder = 10 g/l			
1	1.273	0.674	0.85:2
2	1.293	0.722	0.81:2
3	1.305	0.710	0.83:2
r = 0.4; Surfactant Concentration = 4 g/l; Initial Bulk TiB$_2$ Powder = 10 g/l			
1	0.619	0.491	0.57:2
2	0.534	0.395	0.61:2
3	0.408	0.298	0.62:2

From ICP-AES results, we observed that the stoichiometry of TiB_2 nanosheets increased with the increasing C_S upto 3g/l. At C_S = 4 g/l, we again observe a decrease in Ti atoms. This is expected since the lateral dimensions of nanosheets (<L>) also changes with surfactant concentration. As explained by Coleman and co-workers, <L> shows an increase (similar to nanosheet concentration) with increasing C_S upto a certain concentration and then a decrease in <L>. This indicates that at lower C_S, <L> would be less and hence, lesser presence of Ti atoms. At C_S = 3g/l, nanosheets would have high <L> and hence more presence of Ti atoms (since TiB_2 nanosheets are exfoliated, nanosheets with high <L> have more retention of Ti atoms due to strong Ti-B bond as compared to nanosheets with less <L>). When the C_S increases further, depletion interactions result in settling of larger nanosheets (higher <L>) due to flocculation. This results in the presence of a greater number of nanosheets with less <L> and hence, a decrease in the Ti atom concentration.

M. EPR
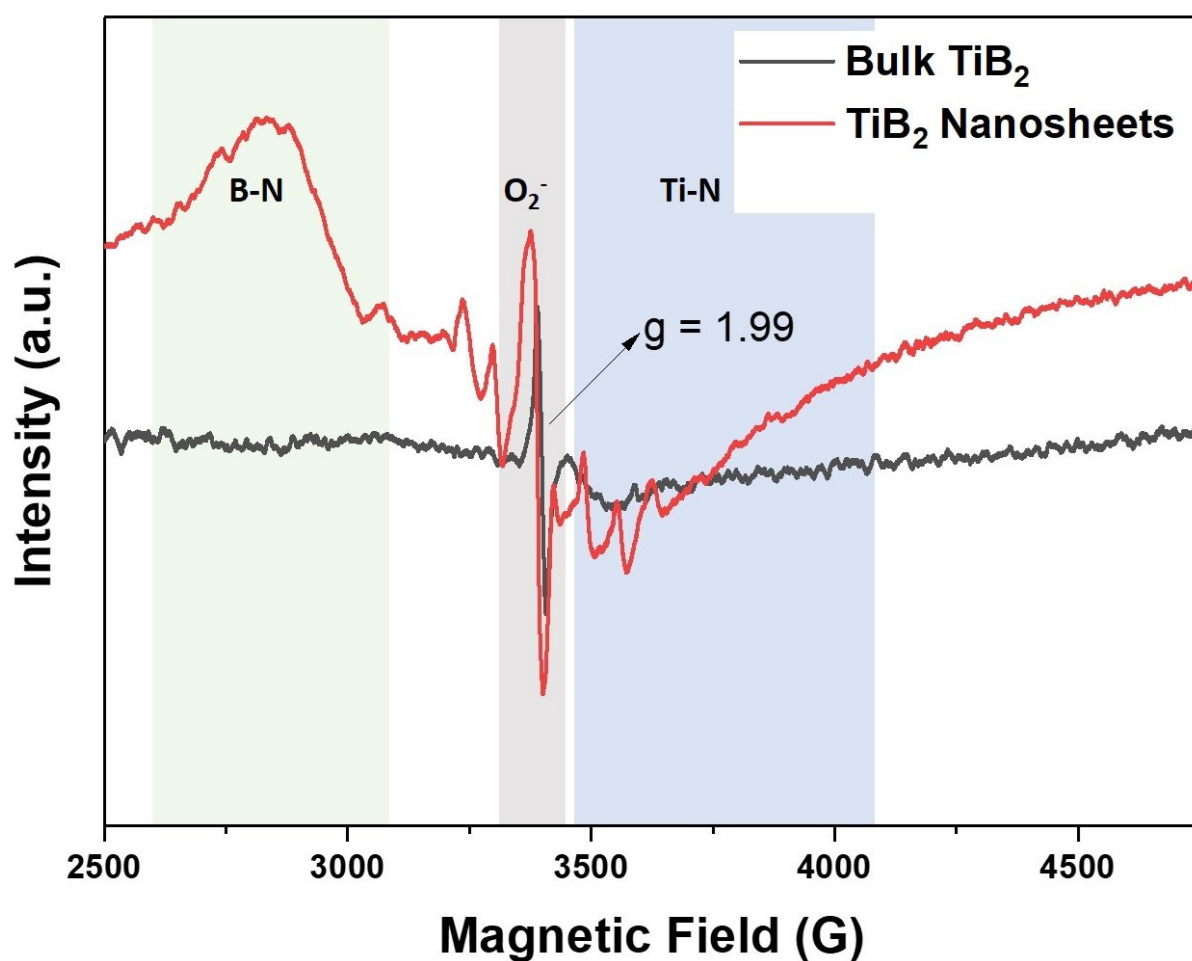
Figure S 22: *EPR spectra of bulk TiB$_2$ and TiB$_2$ nanosheets*

Figure S22 shows the EPR spectra of bulk TiB_2 and TiB_2 nanosheets. Both samples show a strong signal at g factor of ~2 which shows the presence of adsorbed O_2 molecules from the atmosphere. A higher intensity of signal at this point for TiB_2 nanosheets indicates the presence of more defects compared with bulk TiB_2. The increase in the signal at values of g factor > 2 shows presence of Ti-N in the system which is more intense compared with bulk TiB_2. Bodziony *et al.* inferred a similar broadening in the signal for TiN.[9] Similarly, the new signal observed with g factor < 2 shows the presence of B-N in the system that is not present in bulk TiB_2.[10] These results also corroborate with TGA and XPS results.

N. TEM-EDS Plots

TEM – EDS for different nanosheets shows the presence of boron and titanium. In some nanosheets, presence of oxygen is also detected implying that the functionalization cannot be removed completely. The presence of carbon can be due to two reasons – (i) by surfactant, or (ii) by lacey carbon grid, thus having high mass fractions. Similarly, the signal for Cu may be due to the presence of Cu support on the TEM grid. Here, the mass fraction of titanium is far less than boron as compared to boron mass fraction in the other nanosheets. Moreover, there is presence of some nitrogen. This presence has also been noted in the XPS results of the nanosheets mentioned in the main manuscript. Further studies are underway to determine the reasons behind the presence of such nitrogen signals in different characterizations.
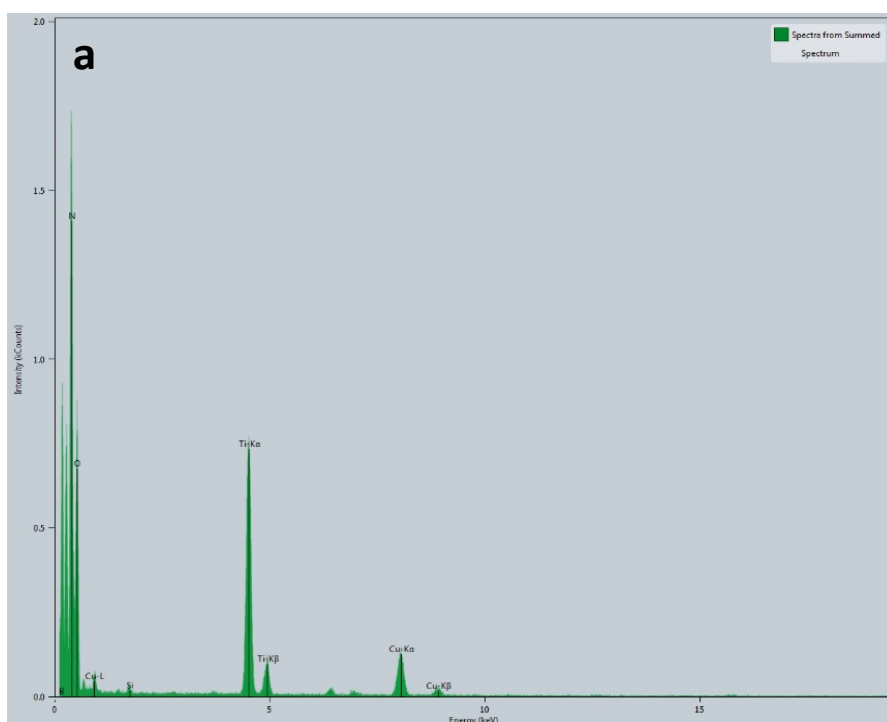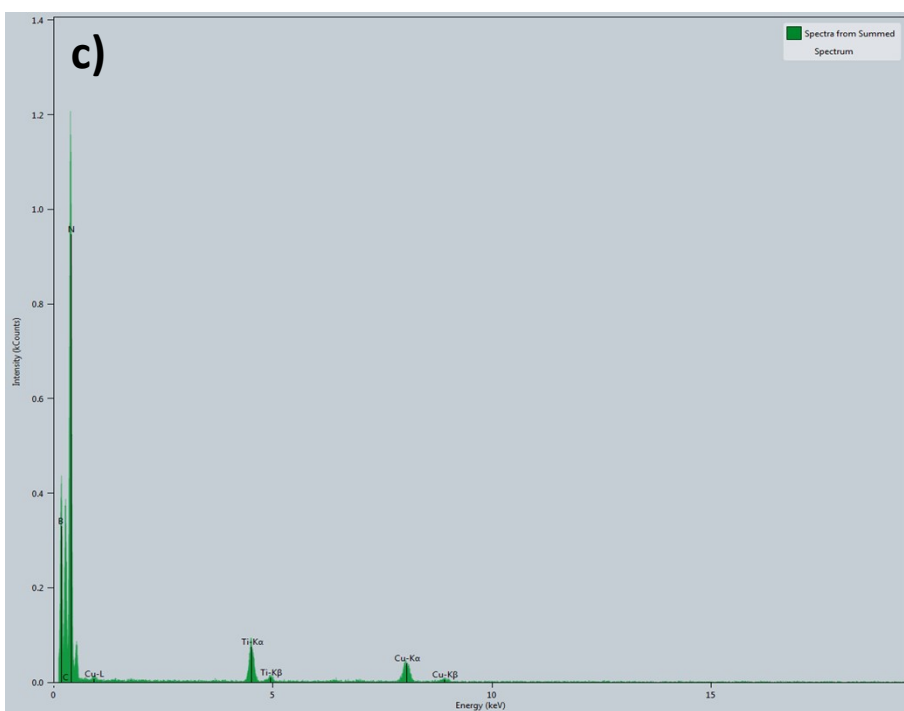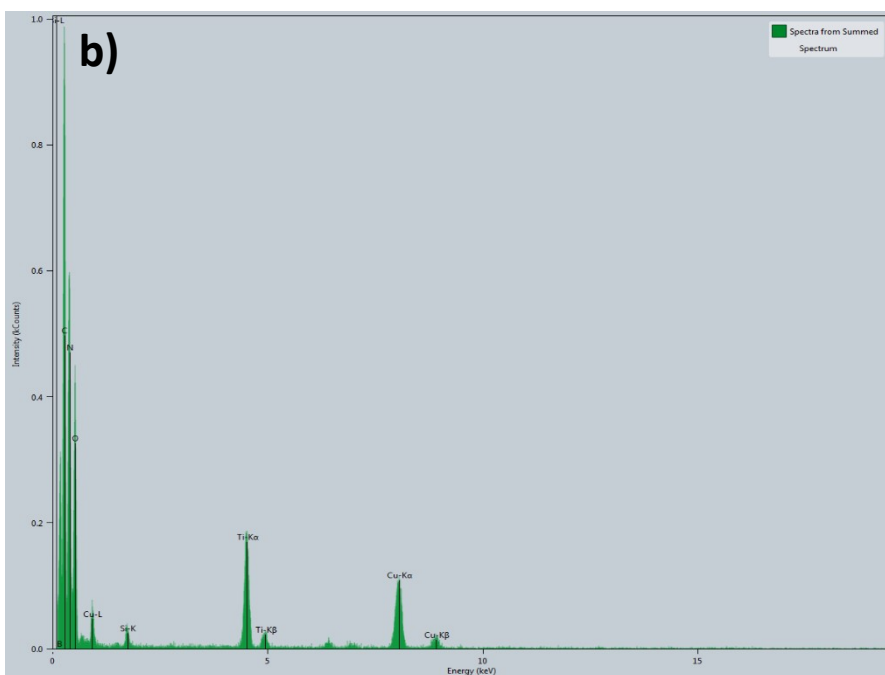
Figure S 23: *TEM-EDS mapping of 3 different nanosheets showing presence of nitrogen*

O. TGA Analysis
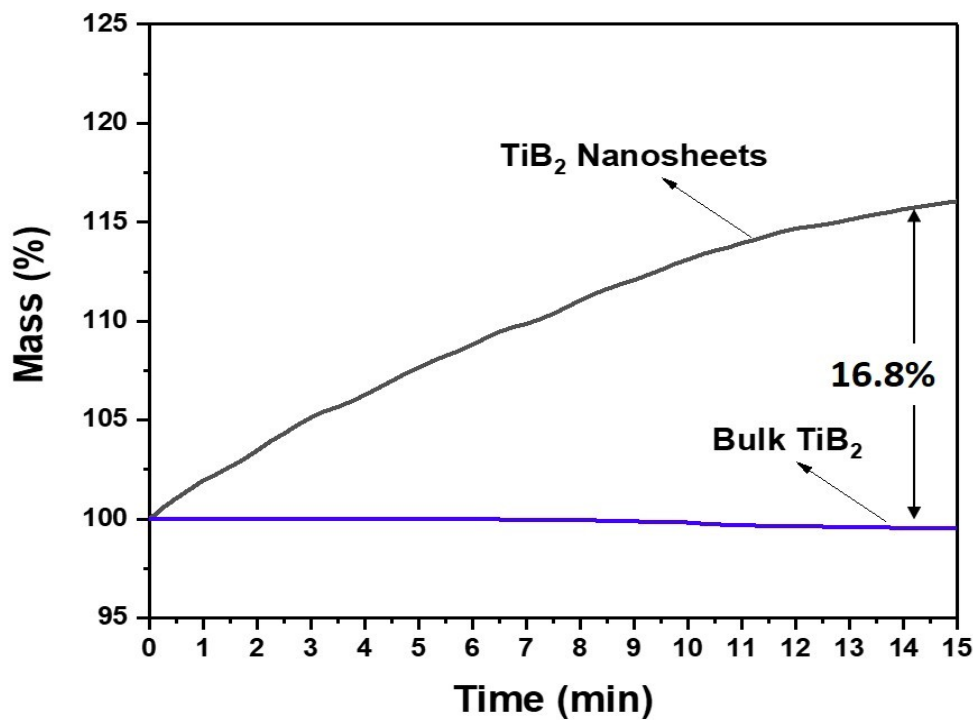
Figure S 24: *Mass change (%) in bulk TiB$_2$ and TiB$_2$ nanosheets with time, when N$_2$ gas is purged at 25℃.*
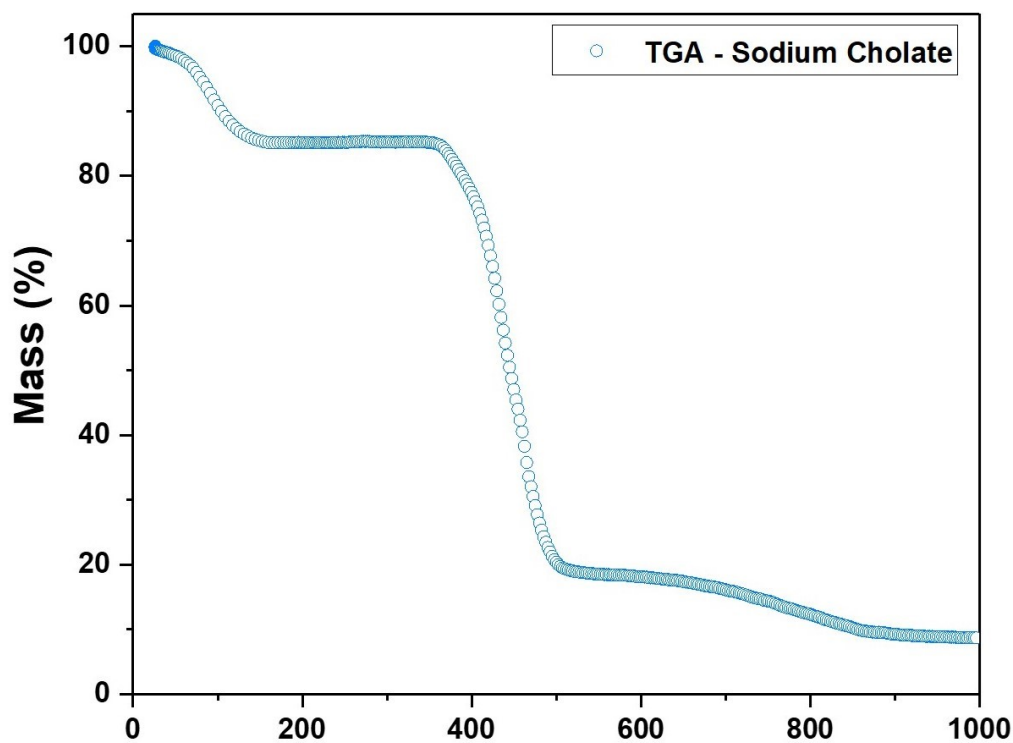
Figure S 25: *Mass change (%) of sodium cholate when temperature is raised to 1000℃*

P. Characterization studies of nanosheets obtained after TGA analysis

1. XRD Studies
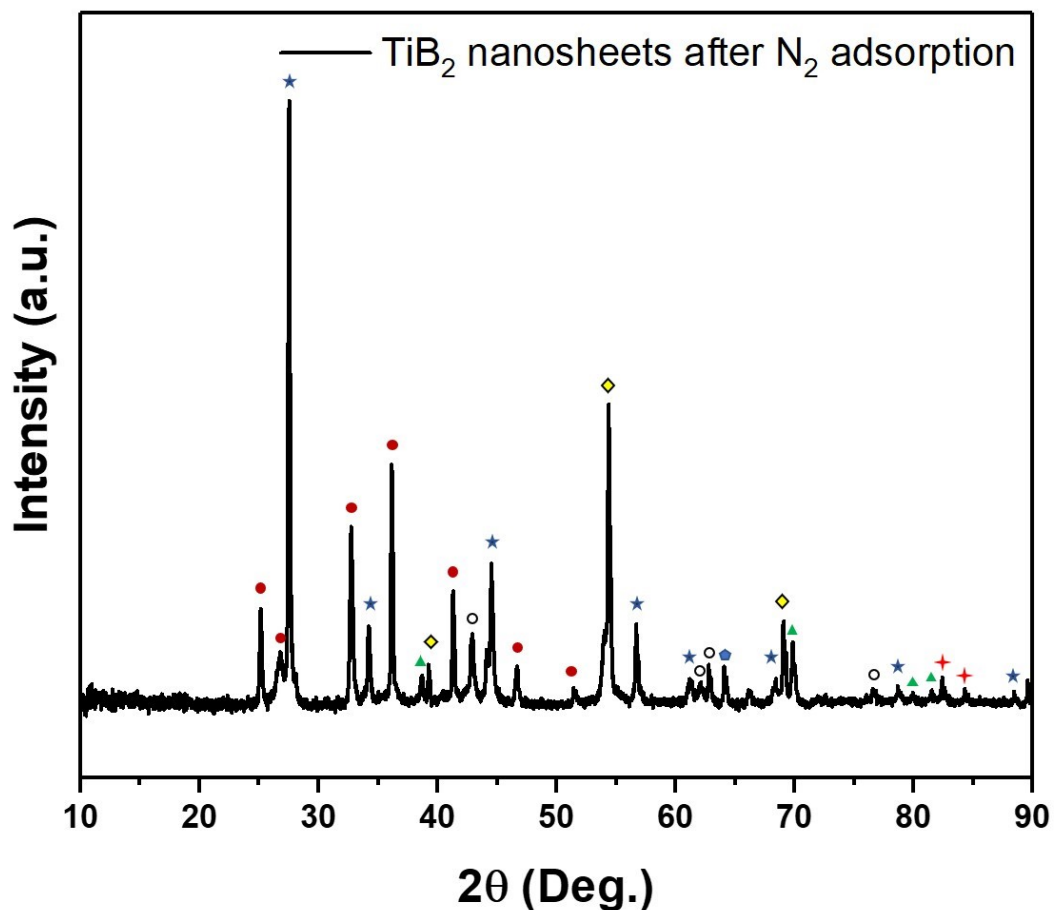
Figure S 26: XRD pattern of TiB_2 nanosheets after N_2 adsorption

Table S 4: Different phases formed after N_2 adsorption along with 2θ values

Symbol	Chemical Formula	2θ (Deg.)	(hkl) values
★	TiB_2 (ICDD - 00-035-0741)	27.5	(001)
		34.2	(100)
		44.4	(101)
		56.9	(002)
		61.2	(110)
		68.3	(111)
		78.6	(201)
		88.3	(112)
●	$TiO_{0.34}N_{0.74}$ (ICDD - 00-044-0951)	25.1	(200)
		26.7	(111)
		32.8	(302)
		36.2	(013)
		41.4	(204)

		46.5	(304)
		51.6	(022)
◇	**BN** (ICDD - 00-018-0251)	39.2	(131)
		54.1	(241)
		69.2	(243)
	TiN_xO_y		
○	$TiN_{0.37}O_{0.51}$ (ICDD – 04-001-8790)	42.8	(200)
		62.1	(220)
	$TiN_{0.24}O_{1.88}$ (ICDD – 04-020-5857)	62.7	(204)
	$TiN_{0.21}O_{0.75}$ (ICDD – 04-006-0203)	76.6	(311)
⬠	**BNO** (ICDD – 00-037-1234)	64.7	(004)
✦	$Ti_{0.68}B_{0.1}N_{0.22}$ (ICDD – 00-014-0052)	82.4	(202)
		84.8	(104)
▲	$TiBO_3$ (ICDD – 00-017-0310)	38.6	(110)
		69.8	(300)
		76.6	(0012)
		79.9	(0210)

We collected XRD data of TiB_2 nanosheets obtained after TGA studies to check if TiB_2 planes were retained after N_2 adsorption. XRD pattern shows that the native lattice structure of TiB_2 nanosheets was retained with major planes (001), (100), and (101) still present. We also found presence of additional phases such as BN and TiN_xO_y. We also identified the presence of few more phases such as $TiBO_3$ and BNO.

2. FTIR Spectroscopy

FTIR spectroscopy further indicated an increase in the amount of adsorbed species i.e., N_2 and O_2 (Figure S27). Two characteristic peaks of BN were observed at 810 cm^{-1} and 1380 cm^{-1} corresponding to out-of-plane vibration of B-N-B bond and in-plane stretching of B-N bond respectively.[11] Similarly, the peak at 654 cm^{-1} corresponds to presence of TiN species that have undergone oxidation.[12,13] Although new peaks emerged in FTIR spectra of TiB_2 nanosheets and further when N_2 adsorption occurred when heated to 1000 °C, the peak at 1641 cm^{-1} diminished.[3,14,15] This peak corresponds to the presence of Ti-OH bond, which diminishes due to nanosheets being subjected to high temperatures. These results corroborated with the phases we obtained from XRD patterns.
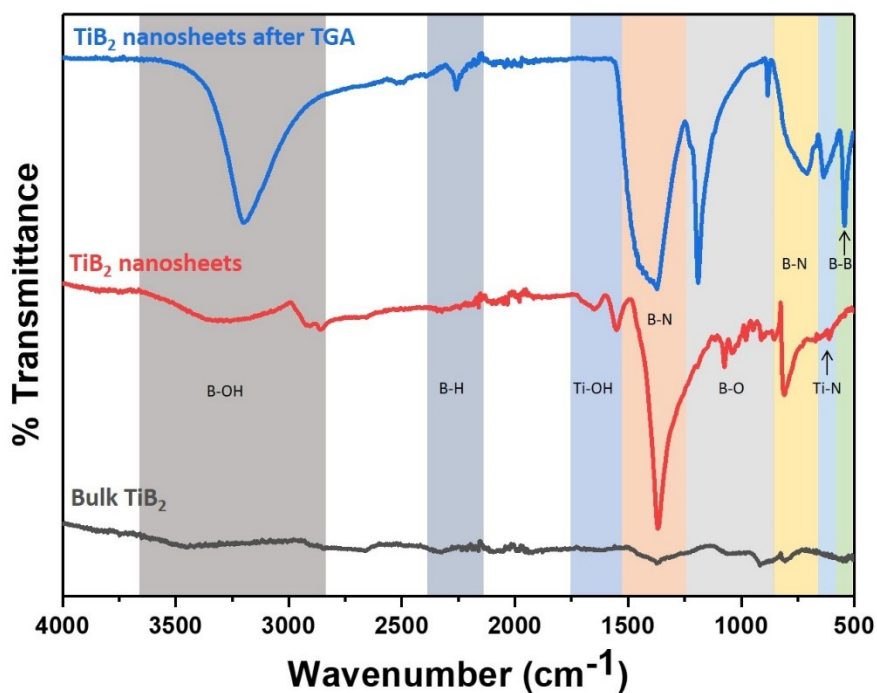
Figure S 27: *FTIR spectra of Bulk TiB₂, TiB₂ nanosheets, and TiB₂ nanosheets after N₂ adsorption as obtained after TGA*
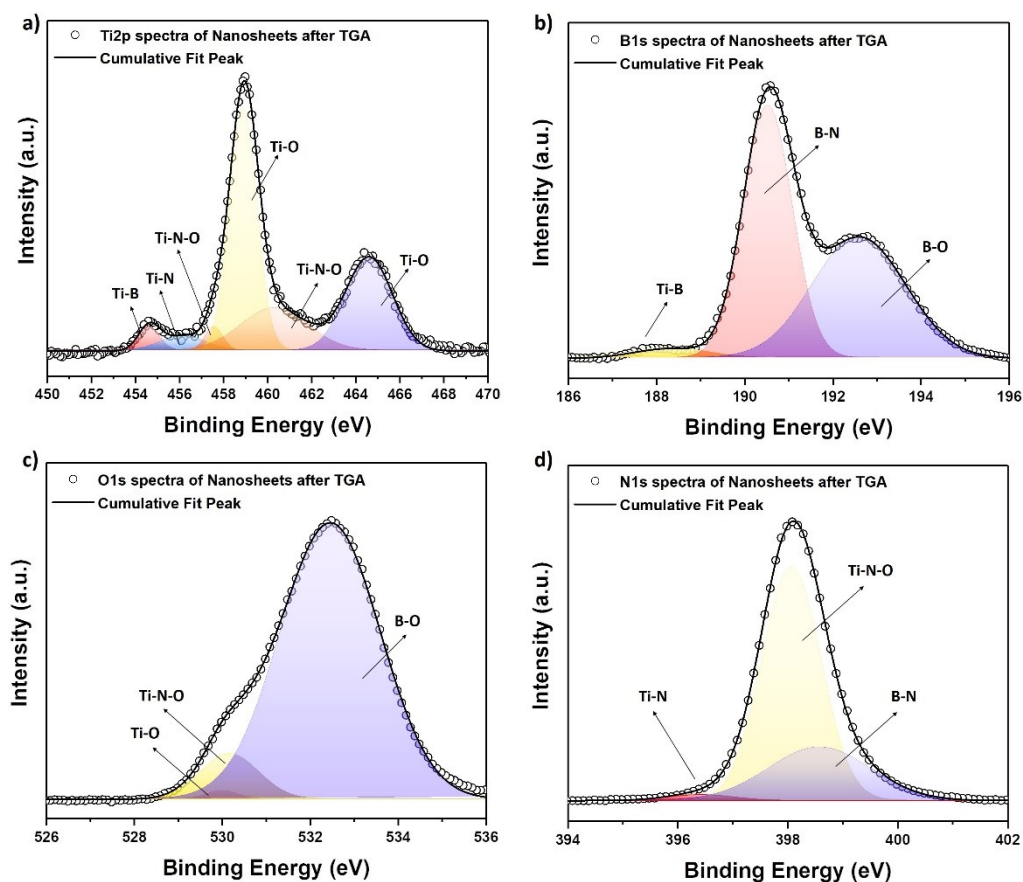
Figure S 28: *(a)Ti2p spectra, (b) B1s spectra, (c) O1s spectra, and (d) N1s spectra of N₂ adsorbed nanosheets acquired by XPS*

To further understand the chemical interface of these TiB_2 nanosheets obtained after TGA, we collected XPS spectra (Figure S28). Ti2p spectra of these nanosheets exhibits six peaks – 454.5 eV (attributed to Ti-B bond), 455.8 eV (attributed to Ti-N bond), 457.4 eV and 460.3 eV (attributed to Ti-N-O bond), 458.8 eV and 464.5 eV (attributed to Ti-O bond).[3,16–19] The presence of these peaks indicates formation of metal nitride phases as observed in XRD pattern (Figure S26).

B1s spectra of N_2 adsorbed nanosheets exhibits similar three peaks at 187.5 eV (attributed to Ti-B bond), 190.1 eV (attributed to B-N bond), and 192.5 eV (attributed to B-O bond).[3,19,20] There was a decrease in the intensity of Ti-B bond and an increase in B-N bond. This is possibly due to increase in the adsorption after temperature increase. The presence of these new peaks confirms the increase in the adsorption of N_2, as observed in TGA studies.

O1s spectra exhibits three peaks at 529.7 eV, 530.2 eV, and 532.5 eV. The peaks at 529.7 eV and 532.5 eV corresponds to Ti-O bond and B-O bond respectively.[3,19] The peak at 530.2 eV is attributed to Ti-N-O bond.[19,21] The decrease in the peak at 529.7 eV and corresponding increase in 530.2 eV peak indicates increase N_2 adsorption at Ti sites and hence, the occurrence of new TiN_xO_y phases in XRD.

N1s spectra of N_2 adsorbed nanosheets also exhibits similar peaks to TiB_2 nanosheets before being subjected to high temperatures i.e., 396.5 eV (attributed to Ti-N bonds), 397.7 eV (attributed to Ti-N-O bonds), and 398.3 eV (attributed to B-N bonds).[16–21] The B-N peak shows higher intensity when compared to TiB_2 nanosheets indicating that both B and Ti sites are prone to N_2 adsorption. The XPS survey spectrum (Figure S21) also shows increase in N_2 percentage from 3 % (in bulk TiB_2) and 8 % (in TiB_2 nanosheets) to 16 % (in N_2 adsorbed nanosheets). These results corroborate with the findings of DFT studies that highlights the mechanism of the adsorption.

Q. DFT Studies

Optimized unit cell and supercell of TiB_2

The optimized unit cell and a 3x3x3 supercell of TiB_2 are shown in Figure S23 below. For subsequent calculations of adsorption energies, either the Ti (0 0 1) or the B (0 0 1) surface was exposed, in either the pristine form, or with defects.
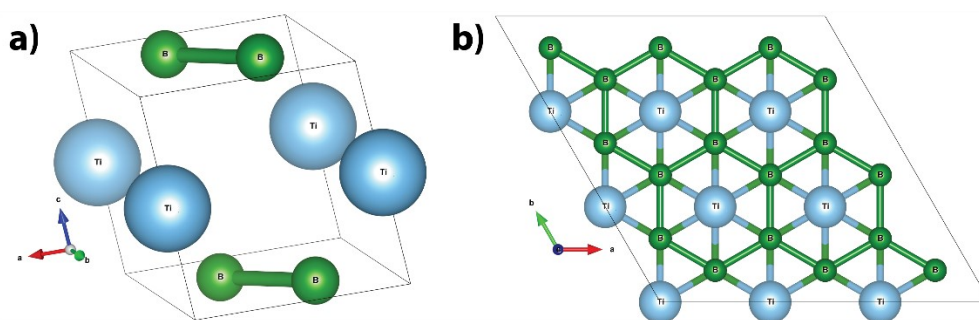
Figure S 29*: (a) optimized unit cell of TiB_2. (b) the top view of a 3x3x3 supercell. The supercell has 81 atoms in total (27 atoms of Ti and 54 atoms of B).*

Simulation of defected surfaces for N_2 adsorption

Figure S24 shows the various types of defects created in the TiB_2 system, for the case where Ti (0 0 1) is the exposed surface for adsorption of N_2. These include monovacant systems containing single vacancies of Ti and B (denoted as T1, T2 for titanium monovacancies; B1, B2, B3 and B4 for boron monovacancies, and a divacant system containing 2 B vacancies (denoted as B1B1). Structures were fully relaxed before calculation of adsorption energies.
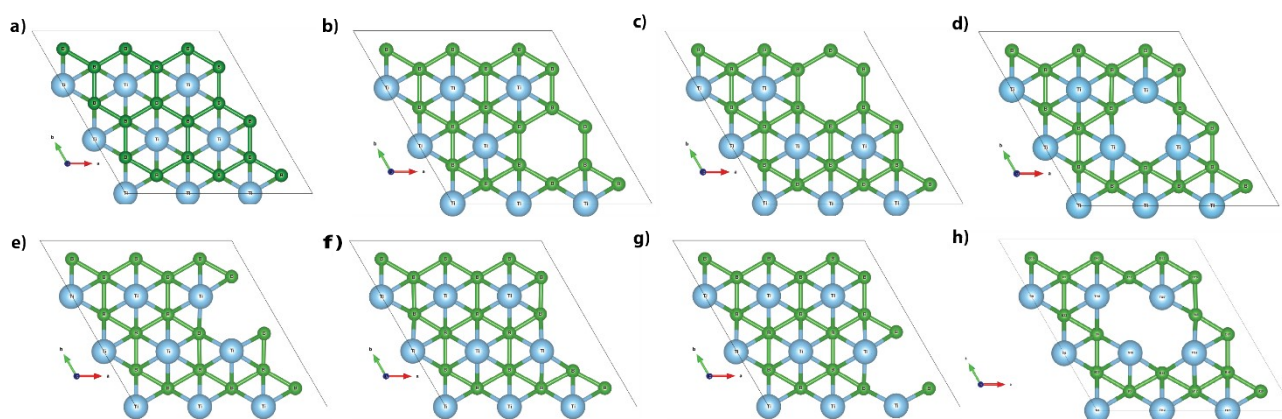
Figure S 30: *Top view of various defected TiB_2 surfaces (here, Ti-(0 0 1) is the exposed surface) used for adsorption studies. Panels represent (a) – pristine, (b) – T1 vacancy, (c) –*

T2 vacancy, (d) – B1 vacancy, (e) – B2 vacancy, (f) – B3 vacancy, (g) – B4 vacancy, (h) – B1B1 (divacancy).

Ground state energies for N_2 adsorption for various surfaces

Table S 5: Ground state energies of various systems with Ti (0 0 1) exposed surface for N_2 adsorption. The last column indicates the adsorption energy for N_2.

No	System (Ti (0 0 1) exposed)	Without-N_2	N_2-adsorbed	ΔE-N_2	ΔE_{avg}-N_2
1	TiB_2	-643.3280	-663.3744	-3.42E+00	-1.265E-01
	Monovacant Systems				
2	$Ti_{0.963}B_2$-T1	-632.5299	-652.0738	-2.91E+00	-1.121E-01
3	$Ti_{0.963}B_2$-T2	-632.5299	-651.9744	-2.81E+00	-1.082E-01
4	$TiB_{1.963}$-B1	-633.0985	-653.6220	-3.89E+00	-1.497E-01
5	$TiB_{1.963}$-B2	-633.0985	-653.1233	-3.39E+00	-1.306E-01
6	$TiB_{1.963}$-B3	-633.0985	-653.1180	-3.39E+00	-1.303E-01
7	$TiB_{1.963}$-B4	-633.0985	-653.0179	-3.29E+00	-1.265E-01
	Divacant System				
8	$TiB_{1.926}$ -B1B1	-626.6684	-644.9109	-4.592E+00	**-1.837E-01**

Table S 6: Ground state energies of various systems with B (0 0 1) exposed surface for N_2 adsorption. The last column indicates the adsorption energy for N_2.

No	System (B (0 0 1) exposed)	Without-N_2	N_2-adsorbed	ΔE-N_2	ΔE_{avg}-N_2
1	TiB_2	-643.6658	-660.4043	-1.08E-01	-3.999E-03
	Monovacant Systems				
2	$Ti_{0.963}B_2$-T1	-629.9189	-646.5565	-7.022E-03	-2.701E-04
3	$Ti_{0.963}B_2$-T2	-629.9189	-646.3393	2.102E-01	8.084E-03
4	$TiB_{1.963}$-B1	-634.4992	-652.0068	-8.771E-01	-3.373E-02
5	$TiB_{1.963}$-B2	-634.4992	-650.9196	2.101E-01	8.081E-03
6	$TiB_{1.963}$-B3	-634.4992	-651.0560	7.365E-02	2.833E-03
7	$TiB_{1.963}$-B4	-634.4992	-650.9144	2.153E-01	8.280E-03
	Divacant System				
8	$TiB_{1.926}$ -B1B1	-626.6684	-649.0224	-5.723E+00	**-2.289E-01**

Bader charge analysis

Table S 7: *Bader charge for various atom Ids corresponding to Ti and B from Figure 5e.*

Atom Id for pristine and N_2-adsorbed TiB_2 surface atoms	Atomic charge	
	TiB_2	TiB_2N_2
Ti15	8.9960	8.6162
Ti18	8.9959	8.7329
Ti24	8.9959	8.7329

Ti27	8.9960	8.6162
B33	3.8890	3.8382
B42	3.7962	3.7204
B45	3.8890	3.8382
B66	3.8890	3.8382
B69	3.8876	3.8119
B78	3.8890	3.8382
N82	-	5.9890
N83	-	5.8509

Adsorption energies of N_2

Table S 8: *Average N_2 adsorption energies for 4 surfaces (2 pristine and 2 with Boron divacant defects), as shown in Figure 6 in the manuscript.*

Species adsorbed	*	N_2
Ti-(0 0 1) top layer	0.0000	-3.4158
Ti-(0 0 1) top layer - B1B1	0.0000	-4.5919
B-(0 0 1) top layer	0.0000	-0.1080
B-(0 0 1) top layer - B1B1	0.0000	-5.7235

References:

1   J. Wang, Y. Xia, Y. Dong, R. Chen, L. Xiang and S. Komarneni, *Appl Catal B*, 2016, **192**, 8–16.

2   X. H. Zhang, N. Li, J. Wu, Y. Z. Zheng and X. Tao, *Appl Catal B*, 2018, **229**, 227–236.

3   A. L. James, M. Lenka, N. Pandey, A. Ojha, A. Kumar, R. Saraswat, P. Thareja, V. Krishnan and K. Jasuja, *Nanoscale*, 2020, **12**, 17121–17131.

4   G. Greczynski and L. Hultman, *Appl Surf Sci*, 2021, **542**, 148599.

5   A. L. James and K. Jasuja, *RSC Adv*, 2017, **7**, 1905–1914.

6   X. Guo, G. Zhang, H. Cui, N. Wei, X. Song, J. Li and J. Tian, *Appl Catal B*, 2017, **217**, 12–20.

7   T. Skaltsas, X. Ke, C. Bittencourt and N. Tagmatarchis, *J Phys Chem C*, 2013, **117**, 23272–23278.

8   Z. Li, R. J. Young, C. Backes, W. Zhao, X. Zhang, A. A. Zhukov, E. Tillotson, A. P. Conlan, F. Ding, S. J. Haigh, K. S. Novoselov and J. N. Coleman, *ACS Nano*, 2020, **14**, 10976–10985.

9   T. Bodziony, N. Guskos, A. Biedunkiewicz, J. Typek, R. Wróbel and M. Maryniak, *Mater Sci Poland*, 2005, 899--907.

10   F. F. Murzakhanov, B. v. Yavkin, G. v. Mamin, S. B. Orlinskii, I. E. Mumdzhi, I. N. Gracheva, B. F. Gabbasov, A. N. Smirnov, V. Y. Davydov and V. A. Soltamov, *Nanomaterials 2021, Vol. 11, Page 1373*, 2021, **11**, 1373.

11   T. Shen, S. Liu, W. Yan and J. Wang, *J Mater Sci*, 2019, **54**, 8852–8859.

12   D. Choi and P. N. Kumta, *J Electrochem Soc*, 2006, **153**, A2298.

13   K. S. Schramke, Y. Qin, J. T. Held, K. A. Mkhoyan and U. R. Kortshagen, *ACS Appl Nano Mater*, 2018, **1**, 2869–2876.

14   G. Gohari, A. Mohammadi, A. Akbari, S. Panahirad, M. R. Dadpour, V. Fotopoulos and S. Kimura, *Scientific Reports 2020 10:1*, 2020, **10**, 1–14.

15   R. Patidar, H. Gunda, A. K. Varma, R. Gawas, S. K. Das and K. Jasuja, *Ceram Int*, 2020, **46**, 28324–28331.

16   S. Jiang, B. Yi, H. Zhang, W. Song, Y. Bai, H. Yu and Z. Shao, *ChemElectroChem*, 2016, **3**, 734–740.

17   Y. Han, X. Yue, Y. Jin, X. Huang and P. K. Shen, *J Mater Chem A Mater*, 2016, **4**, 3673–3677.

18   E. O. Filatova, S. S. Sakhonenkov, A. S. Konashuk, S. A. Kasatikov and V. V. Afanas'Ev, *J Phys Chem C*, 2019, **123**, 22335–22344.

19   G. M. National Institute of Standards and Technology, NIST X-ray Photoelectron Spectroscopy Database, NIST Standard Reference Database Number 20.

20   Q. Liu, C. Chen, M. Du, Y. Wu, C. Ren, K. Ding, M. Song and C. Huang, *ACS Appl Nano Mater*, 2018, **1**, 4566–4575.

21   A. Hinckley and A. Muscat, *Solid State Phenomena*, 2018, **282**, 232–237.